Journal of Engineering Science 14(2), 2023, 69-77
DOI: https://doi.org/10.3329/jes.v14i2.71229

JES
an international Journal

MANGANESE OXIDE BASED CORE@SHELL NANOPARTICLES AND ITS APPLICATION IN AQUEOUS ZINC-ION BATTERY

Rabeya Sultana Mim[1], Md. Ibrahim Hossain Mollah[1], Rakhi Kundu[1], Nusrat Tazeen Tonu[1], Md. Mahfujul Hasan[2], Md. Saddam Hossain[1], Mohammad Abu Yousuf[1] and Parbhej Ahamed[*1]

[1]*Department of Chemistry, Khulna University of Engineering & Technology (KUET), Khulna-9203, Bangladesh*
[2]*Institute of Food Science & Technology (IFST), Bangladesh Council of Scientific and Industrial Research (BCSIR), Dhanmondi, Dhaka-1205, Bangladesh*

Received: 24 July 2023 Accepted: 18 November 2023

ABSTRACT

In this study, MnO_2 as well as core@shell type MnO_2@Ag material were prepared through the versatile reverse micelle route. FTIR absorption band at 522 cm^{-1} was ascribed to the Mn-O stretching mode, demonstrating the presence of a Mn-O bond inside the MnO_2 structure. XRD was used to determine the crystalline structure of the prepared samples. Peaks at 2θ = 12.7°, 18.1°, 28.8°, 37.5°, 42.1°, 49.9°, 56.2°, and 60.3° matched the α-MnO_2 diffraction peaks nicely. The spherical shape of the produced MnO_2 and MnO_2@Ag compounds was observed in FESEM. The results of the histogram show that MnO2@Ag particles are marginally smaller than MnO2 particles. The electrochemical assessment of the generated cathode materials for aqueous zinc-ion battery (AZIB) CR-2032 was conducted using cyclic voltammetry (CV), electrochemical impedance spectroscopy (EIS), and battery charge-discharge (BCD) techniques.

Keywords: *Manganese dioxide, Micro-emulsion technique, Zinc-ion battery.*

1. INTRODUCTION

Energy resources push the current techno-sphere of a realm to drive today's society into a new tomorrow's one. They act as a lung for the global modern economy of a country. Issue of economic growth of a country entirely depends on the degree of energy consumption. However, the pattern of unsustainable consumption of non-renewable energy resources such as coal, natural gas, oil *etc.* and subsequent environment deterioration nature have been triggered us to use renewable energy resources (Karden *et al*., 2007; Tran *et al*., 2021). Among various sustainable energy resources the availability of solar, wind and water are discontinuous. Because of this intermittent behaviour of solar, wind and water resources scientists around the world are in the quest of effective mediums for storing and transferring energy upon necessity (Panchal *et al*., 2016; Parker *et al*., 2017). The development of energy storage devices are an urgent need for the continuous consumption of renewable energy resources. Accordingly, the advent of various types of storage technologies such as lead-acid batteries, nickel-cadmium batteries, lithium ion batteries and nickel-metal hydride batteries have been provided hope and viable solutions associated with renewable resources. The inherent constraints of these mediums have been limited their potential applications in large-scale energy storage systems. Therefore, finding ways to overcome the shortcomings of those battery systems make up aqueous rechargeable batteries device (ARBD). Aqueous solution of salt acts as an electrolyte in aqueous battery. Natures of the aqueous solutions of salt ensure several advantages such as cheapness, high security and environment benignity compared to non-aqueous batteries. In addition, the high ionic conductivity of aqueous solutions of salt greatly improved the rate capability and performance of the ARBD.

So far, many research groups have done their pioneering work in the direction of ARBD. Among these candidates for aqueous rechargeable batteries, aqueous zinc ion batteries (AZIBs) paved outstanding wave of research direction with full of vitality since the first development of $Zn/ZnSO_4/MnO_2$ system by Yamamoto *et al.* in 1986 (Li *et al*., 2018). Afterwards, tremendous studies have been made for the development of AZIBs. Some pioneering works have been shown significant advances to achieve high capacity and acceptable energy density of AZIBs. Their successes have been encouraged to develop cathode materials such as manganese-based oxides [Wan et al., 2018], vanadium-based materials (Hao *et al*., 2019) and Prussian blue analogue (Maccario *et al*., 2008) for low cost, high safety, long cycle life and environmentally friendly AZIBs with more efforts. Subsequent strategies such as compositing of conductive materials, construction of nanostructure materials, defect introduction and interlayer spacing adjustment of the existing materials have been the hot topics to

*Corresponding Author: *parbhej@chem.kuet.ac.bd*

ISSN 2075-4914 (print); ISSN 2706-6835 (online)

implement the transition of AZIBs from laboratory to commercialization (Li *et al*., 2017). AZIBs research based on those strategies concern insights to delve many elusive obstacles such as dendrite formation, low coloumbic efficiency and poor reversibility (Luo *et al*., 2017). Strategies to overcome the aforementioned bottleneck for the potential commercial applications inspire us to coat manganese dioxide (MnO_2) using conductive silver (Ag) metal. Compared to MnO_2 electrode material alone, there is a clear benefit to the combination of MnO_2 and metallic Ag in terms of improved electrical conductivity. In this study, core@shell type MnO_2@Ag material has been prepared through the versatile reverse micelle route and applied as cathode material for rechargeable AZIBs.

2. MATERIALS AND METHODS

Materials and chemicals for the experimental operations were bought from a number of chemical companies. The materials and chemicals purchased were all laboratory grade and were used without additional purification. The methodology of the study consists of two parts. At first, core shell MnO_2@Ag materials has been prepared using water in oil micro-emulsion technique and its characterization. Next step consists of the fabrication of CR-2032 coil cell using the prepared MnO_2@Ag material.

(i) Methodology for the synthesis of MnO_2@Ag material

Triton X-100, cyclohexanol, and cyclohexane were utilized as surfactant, co-surfactant, and oil phase, respectively, in the synthesis of reverse micelles. 20 mL cyclohexane, 12 mL Triton-X 100, and 8 mL cyclohexanol were combined in a beaker in a 5:3:2 ratio to make the micro-emulsion, which was then magnetically stirred continuously until it was transparent. 4 mL water was added to the transparent micro-emulsion solution and stirred for a while. Four stoppered flasks were filled with equal volumes of micro-emulsion solution. In an analytical balance, 0.002 mol $Na_2S_2O_3.5H_2O$ and 0.0053 mol $KMnO_4$ were weighed, and poured into two separate stoppered flasks containing micro-emulsion. After that, each stoppered flask was magnetically stirred for 1 hour. $Na_2S_2O_3.5H_2O$ incorporated micro-emulsion was then added dropwise into micro-emulsion containing $KMnO_4$. The resultant mixture was then magnetically stirred for 12 hours to produce MnO_2, resulting in blackish MnO_2. The reaction can be represented by the following equation.

$$8KMnO_4+H_2O+3Na_2S_2O_3 \longrightarrow 8MnO_2 + 3\ Na_2S_2O_4 + 3\ K_2SO_4+2\ KOH$$

(ii) Preparation of 5% MnO_2@Ag

MnO_2 was initially prepared in micro-emulsion using the process described above. 0.363g $AgNO_3$ and 0.0081 $NaBH_4$ was weighed in an analytical balance. Then the weighed $AgNO_3$ and $NaBH_4$ were poured into another two separate stoppered flasks which containing micro-emulsion solution. Then micro-emulsion having $AgNO_3$ was transferred to the flask containing MnO_2 particles. It was then followed by the addition of $NaBH_4$ from another flask. $AgNO_3$ was reduced and formed shell over the prepared MnO_2 particles. The reaction was magnetically stir for 12 hours and finally MnO_2@Ag was formed. The reaction between $AgNo_3$ and $NaBH_4$ can be represented as follows.

$$AgNO_3 + NaBH_4 = Ag + H_2 + B_2H_6 + NaNO_3$$

After completing the reaction, the micro-emulsion containing MnO_2@Ag was filtered. The filtered product was dried in the oven for 4 hours. To obtain the final product, the substance was placed in a crucible and calcined at 300°C for 4 hours.

(iii) Methodology for the fabrication of CR-2032 coin cell and its characterization

CR-2032 cell was fabricated as coin cell. In a separately, the cathode electrode was prepared by mixing MnO_2/MnO_2@Ag, carbon black, and polyvinylidene fluoride at the weight ratio of 8:1:1. N-methyl pyrrolidine was used to prepare the slurry of the mixture. The prepared slurry was coated on stainless steel plate and dried at 80℃. 3M $ZnSO_4$ was used as electrolyte. Filter paper was used as separator. Zinc foil was used as anode. Along with them other components like spacer, ring and case were used to fabricate CR-2032 coin cell. Biologic sp-300 electrochemical workstation was used to study the electrochemical properties such as specific capacity, electrochemical impedance spectroscopy and cyclic voltammetry of the prepared CR-2032 coin cell.

3. RESULTS AND DISCUSSIONS

3.1 X-ray Diffraction Analysis

Figure 1 shows a schematic representation of the micro-emulsion technique utilized to prepare MnO_2 and MnO_2@Ag materials. $KMnO_4$ has been encapsulated within the pores of the reverse micelle core in one micro-emulsion. Another reactant, $Na_2S_2O_3.5H_20$, was encapsulated within the pores of a reverse micelle core also. MnO_2 was produced after the two reactants were mixed and stirred together. $AgNO_3$ and $NaBH_4$ were added to the synthesized MnO_2 encapsulated in the reverse micelle pore to make MnO_2@Ag core@shell nanoparticles. The reaction mixture was filtered, yielding a brown-colored MnO_2@Ag product. After that, the product was calcined at 300 ^oC and stored in a vial. At the same reaction conditions, bare MnO_2 (without the addition of $AgNO_3$ and $NaBH_4$) was made for comparison. For characterization of the produced MnO_2 and MnO_2@Ag materials, a number of tests including UV-visible spectroscopy, FT-IR, FESEM, XRD, EDS, , and electrochemical characterization were used.

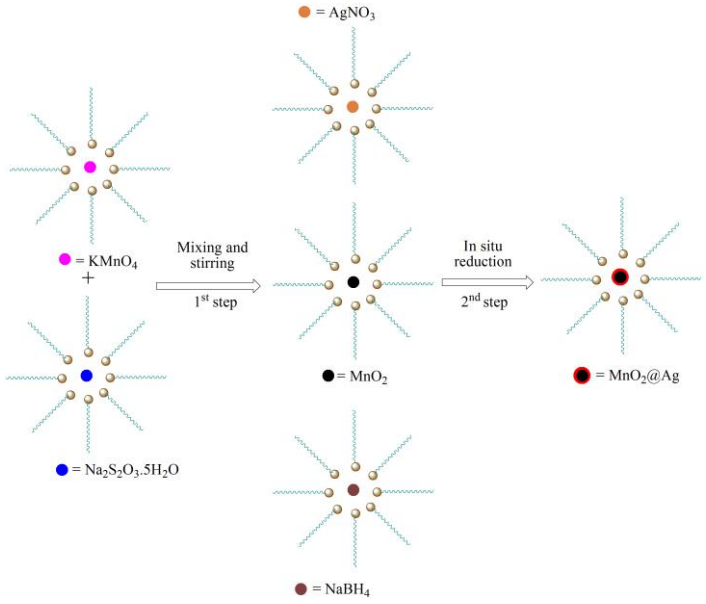

Figure 1: Schematic illustration of the preparation MnO_2 and MnO_2@Ag core shell nano-materials.

3.1 FTIR-Analysis

The FTIR spectra of MnO_2 within the wavenumber ranges from 400 to 4000 cm^{-1} has been shown in Figure 2. The peak at 522 cm^{-1}, which is attributed to the Mn-O bond, appears to be intensifying (Karnchanawong *et al*., 2009; Xará *et al*., 2009). The Mn-O stretching mode can be assigned to the strong absorption band at 522 cm^{-1}, confirming the presence of a Mn-O bond inside the MnO_2 structure.

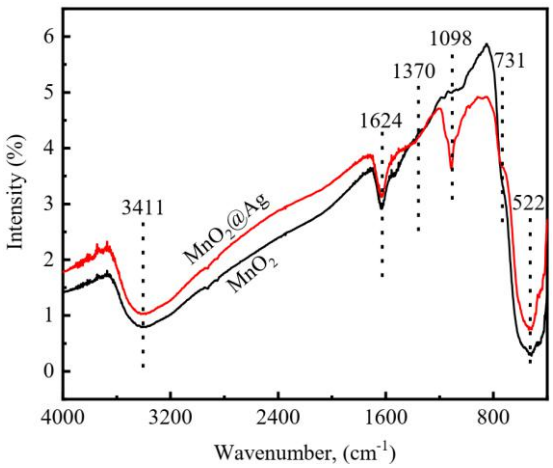

Figure 2: FTIR spectrum shown by the prepared sample.

The O-H bending vibrations combined with Mn atoms correspond to the absorption bands at 731 cm^{-1} and 1370 cm^{-1}.The presence of absorbed water molecules in the MnO_2 (1624 cm^{-1} and 3411 cm^{-1}) structure is suggested by the presence of O-H vibrations in the FTIR spectrum. MnO_2 hydrated characteristics may enrich cation diffusion, hence boosting MnO_2 capacitance (Belardi *et al*., 2011; Sait *et al*., 2014).

3.3 XRD-Analysis

Figures 3(a) and 3(b) depict the XRD patterns of the prepared MnO_2 and MnO_2@Ag materials respectively. The crystalline structure of the two samples was similar, as indicated. The diffraction peaks at 2θ = 12.7°, 18.1°, 28.8°, 37.5°, 42.1°, 49.9°, 56.2°, and 60.3° corresponded well with the diffraction peaks of the α-MnO_2 standard data at (110), (200), (310), (211), (301), (411), (600), and (521) (JCPDS card PDF file no. 44-0141). The micro-emulsion method appears to have produced crystalline MnO_2 and MnO_2@Ag as evidenced by the XRD pattern.

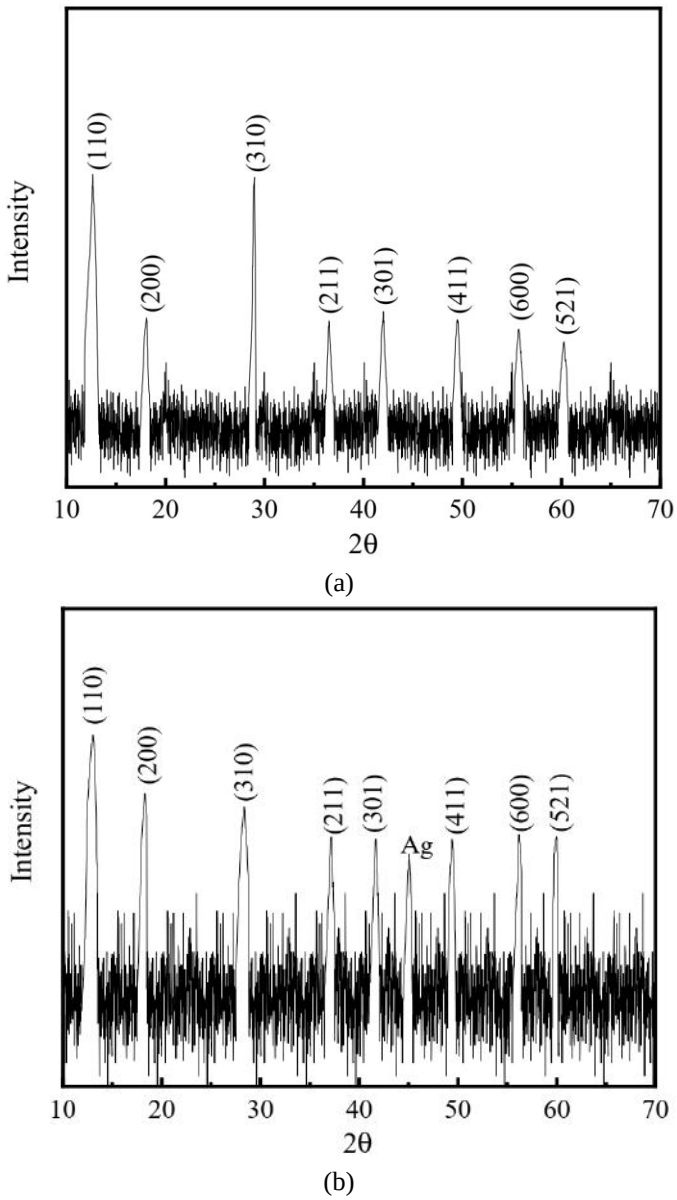

Figure 3: XRD patterns of the prepared (a) MnO_2 and (b) MnO_2@Ag samples.

3.4 FESEM Analysis

The shape and particle size of the produced MnO_2 and MnO_2@Ag materials are investigated using field emission scanning electron microscopy. Figure 4 (a) and (c) illustrates the shape of the prepared MnO_2 and MnO_2@Ag materials respectively. The corresponding particle size distribution are represented in Figure 4 (b) and (d) respectively. The produced MnO_2 materials are spherical in shape, with an average size of 52 nm, as

shown in Figure 4 (a). The particles MnO_2@Ag, on the other hand, are slightly smaller and have a similar form. From the perspective of an Ag sphere on the surface of MnO_2 materials, this observation makes sense.

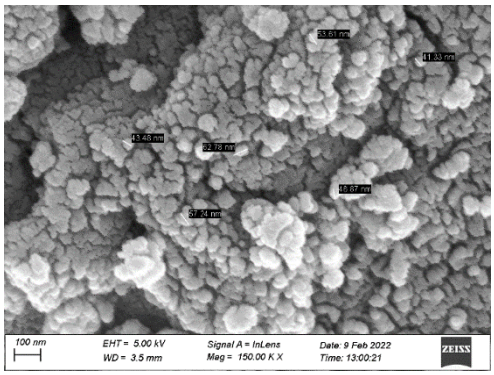

(a) FESEM images of MnO_2

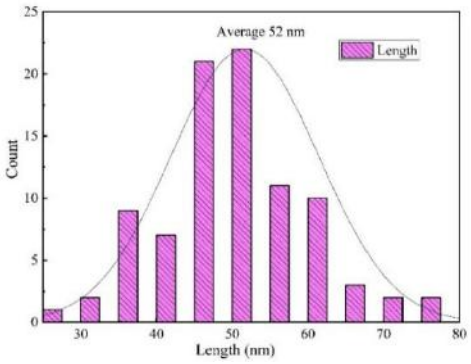

(b) Histogram of image (a)

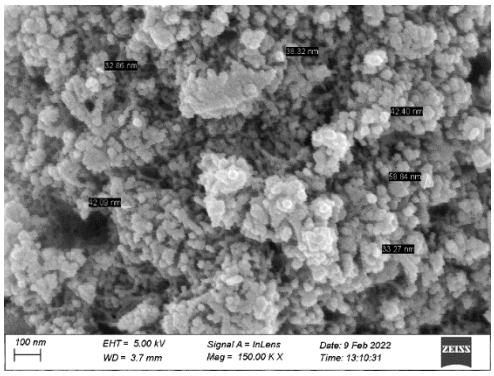

(c) FESEM images of MnO_2@Ag

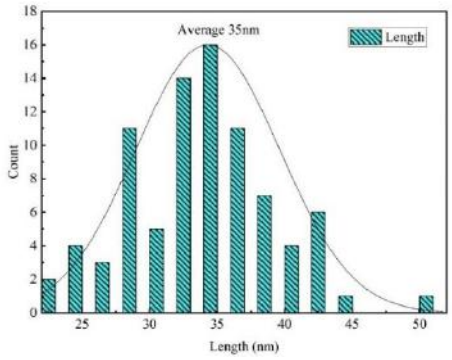

(d) Histogram of image (c)

Figure 4. FESEM images and corresponding histogram of the prepared MnO_2 and MnO_2@Ag materials.

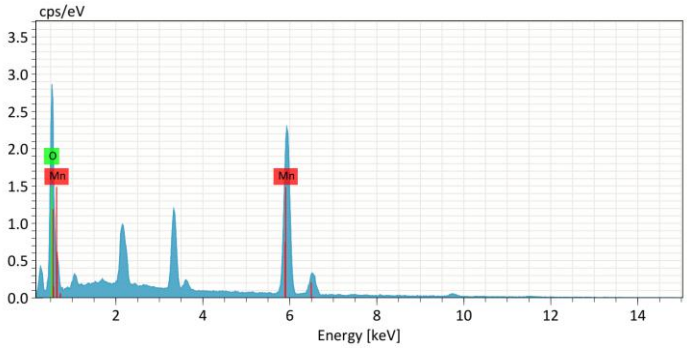

(a) EDS spectrum of MnO_2

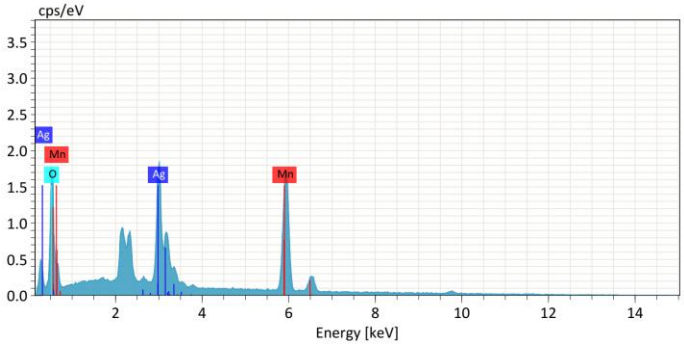

(b) EDS spectrum of MnO_2@Ag

Figure 5: EDS spectrum of the prepared (a) MnO_2 and (b) MnO_2@Ag materials.

3.5 EDS Analysis

The EDX of the nanoparticles MnO_2 and MnO_2@Ag is shown in Figure 5 (a) and 5 (b) respectively. It indicates that the prepared nanoparticles are primarily made up of MnO_2. In the EDS spectrum 5(b), the element Ag is found. This indicates that the substance MnO_2@Ag is manufactured. The remnants of K signal in this image are impurities left over from the reactions. Carbon tap sample holder is responsible for the C signal in this image. Because the elements K and C are present in trace levels in the metal oxide samples, they cannot be detected as new phases in the XRD pattern.

3.6 Electrochemical Characterization

Coin cells were used to test the electrochemical performance of the prepared samples MnO_2 and MnO_2@Ag samples. The coin cells CR-2032 were fabricated and tested using the synthesized cathode material. This section goes into the specifics of several electrochemical characterizations.

3.6.1 Cyclic Voltammetry (CV) of CR-2032 Coin Cell Using MnO_2 Cathode Material

The CV curves of the MnO_2-Zn cell is shown in Fig. 6. An electrochemical window of 1.0-2.1 and a scan rate of 5 mV/s were used to run the cyclic voltammetric scan. At 1.7903 V and 1.2331 V, two pairs of reversible redox peaks can be clearly seen. A two-step reaction can be represented by these two peaks [Zhao et al., 2018 & Sun et al., 2017]. An anodic peak at 1.7903 V and a cathodic peak at 1.2331 V are observed at first cycle of the fresh battery. The phase of Zn^{2+} extraction can be represented by the anodic peak. The cathodic peak can be used to determine the phase of Zn^{2+} insertion. The acquired CV profiles are similar to an approximate those of previously reported α-MnO_2, showing that the synthesized MnO_2 may use the same charge storage mechanism as previously reported α-MnO_2 [Chen et al., 2020 & Gao et al., 2020].

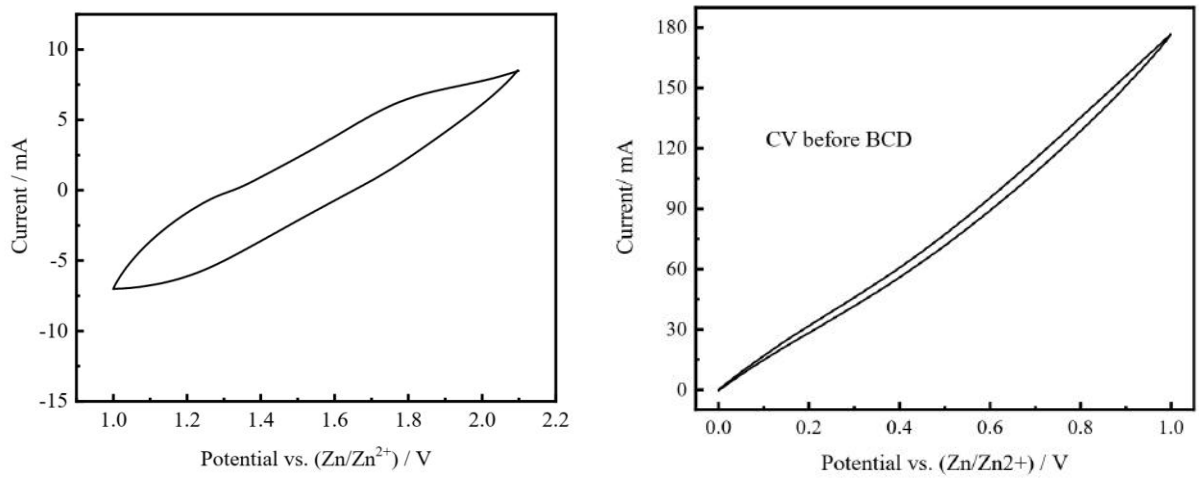

(a) (b)

Figure 6: CV plot of coin cell using (a) MnO_2 (b) MnO_2@Ag cathode materials at 5 mV/s.

3.6.2 Battery Charge Discharge

Figures 7 (a) and 7 (b) show the cycling performances of MnO_2 and MnO_2@Ag samples at 250 µA respectively. The charge/discharge profiles are consistent with the CV profiles as shown in Figure 6. Both type of batteries were cycled up to 20 cycles. MnO_2 and MnO_2@Ag samples have initial charge capacities of 126 mAh and 115 mAh, respectively. MnO_2 and MnO_2@Ag samples have initial discharge capacities of 140 mAh and 203 mAh, respectively. Hence, MnO_2@Ag samples have a larger initial discharge capacity than bare MnO_2, which can be attributed to the Ag coating on MnO_2. After 20 cycles, the capacity of MnO_2 batteries has been found to be nearly constant.

After the eighth cycle, however, the charging capacity of Ag coated MnO_2 dropped by 16 % and the discharging capacity dropped by 18 %. Following that, capacity remains nearly constant for the remainder of the cycles. Initially, the Ag coating on MnO_2 can be accountable for the greater charge and discharge capabilities of MnO_2@Ag. The disintegration of the Ag coating from the MnO_2 surface could explain the sudden attenuation of

MnO_2@Ag after the eighth cycle. Sudden capacity attenuation of MnO_2@Ag may have resulted from the dissolution of Mn from MnO_2. Overall, the MnO_2@Ag electrode has a higher capacity than the MnO_2 electrode.

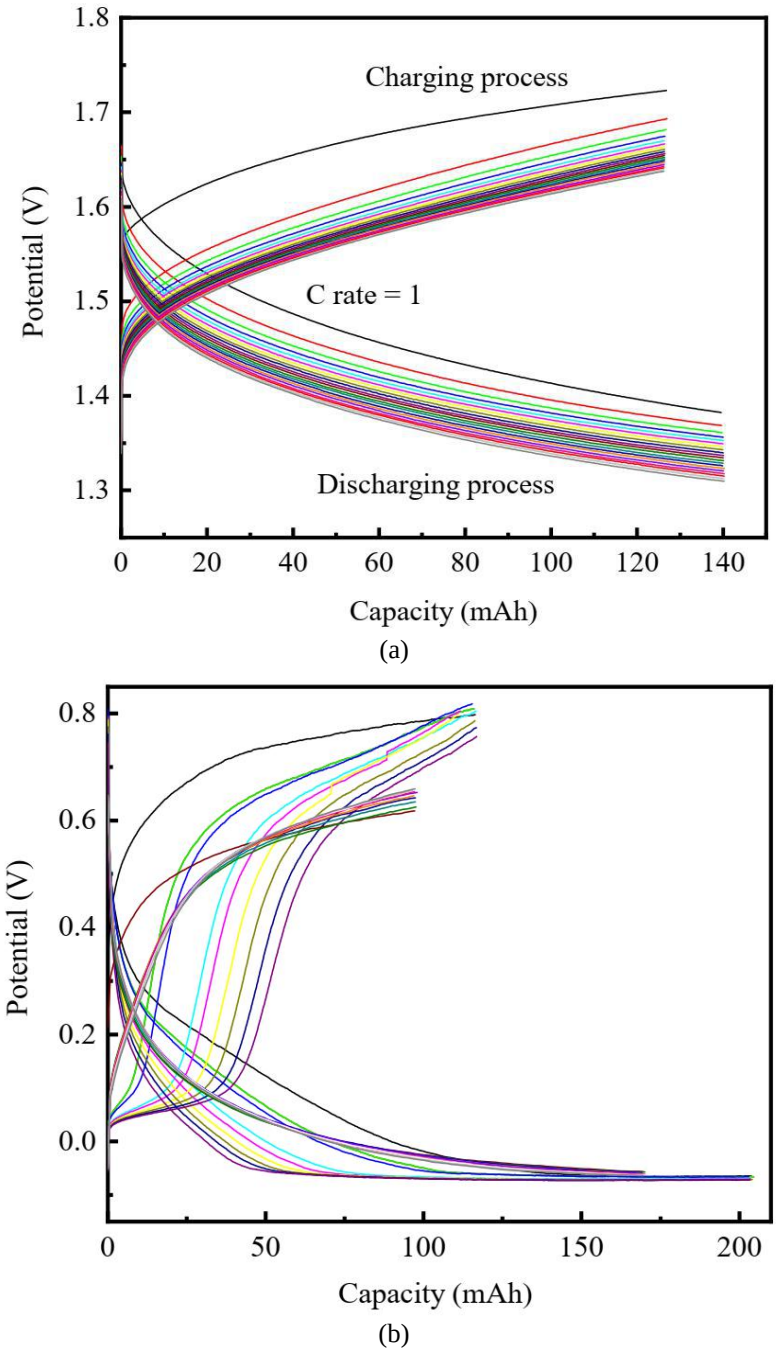

Figure 7: Cycling performances of (a) MnO_2 and (b) MnO_2@Ag samples.

3.6.3 Potentio Electrochemical Impedance Spectroscopy (PEIS) of MnO_2 and MnO_2@Ag

PEIS analysis was used to determine the impedance of MnO_2 and MnO_2@Ag electrodes. PEIS measurements for MnO_2 and MnO_2@Ag electrodes are shown in Figure 8 (a) and Figure 8 (b), respectively. According to the fitting results, the resistance of MnO_2@Ag is lower than that of MnO_2. Before BCD profiles, the R_s value of MnO_2 electrode is 88 ohm. The R_s value of MnO_2@Ag electrode is 37.6 ohm. The reduction in resistance of MnO_2@Ag is due to the Ag coating on the MnO_2 electrode. MnO_2@Ag electrodes with Ag coating may have better electron and ion conductivity. It may have improved wettability and electrode-electrolyte contact surface.

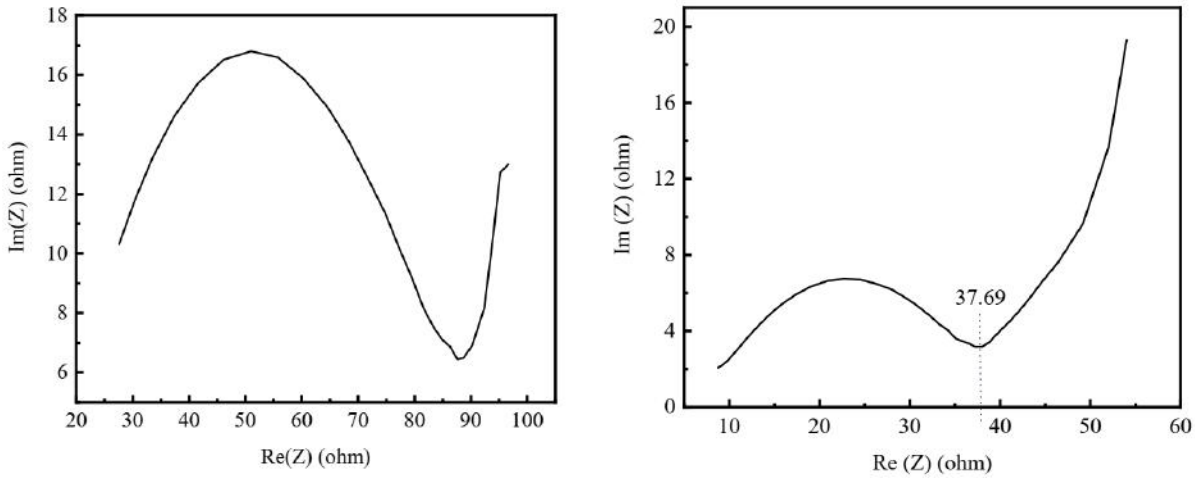

(a) (b)

Figure 8: PEIS analysis of CR-2032 coin cell using materials (a) MnO_2 (a) MnO_2@Ag.

4. CONCLUSIONS

This study shows a straightforward, scalable, and cost-effective method for producing MnO_2 and MnO_2@Ag cathode materials using micro-emulsion technique. The nanostructured MnO_2 and MnO_2@Ag cathode materials were then characterized and used as cathodes for rechargeable zinc ion batteries. The effect of an Ag coating on the surface of MnO_2 was thoroughly investigated. This study found that Ag coating on MnO_2 nanoparticles can have better electrochemical performance than bare MnO_2. As a result, Ag coating on MnO_2 is a good technique to create MnO_2@Ag cathode materials for Zn/MnO_2@Ag ARB construction.

CONFLICT OF INTEREST

The authors declare that they have no conflict of interest.

REFERENCES

Belardi, G. Ballirano, P. Ferrini, M. Lavecchia, R. Medici, F. Piga, L. & Scoppettuolo, A., 2011, "Characterization of spent zinc–carbon and alkaline batteries by SEM-EDS, TGA/DTA and XRPD analysis". *Thermochimica Acta*, Vol. 526(1-2), pp. 169-177.

Chen, M. Zhou, W. Wang, A. Huang, A. Chen, J. Xu, J. & Wong, C. P., 2020, "Anti-freezing flexible aqueous Zn–MnO_2 batteries working at− 35 C enabled by a borax-crosslinked polyvinyl alcohol/glycerol gel electrolyte". *Journal of Materials Chemistry A*, Vol. 8(14), pp. 6828-6841.

Gao, X. Wu, H. Li, W. Tian, Y. Zhang, Y. Wu, H. & Ji, X., 2020, "H^+-insertion boosted α-MnO_2 for an aqueous Zn-ion battery". *Small*, Vol. 16(5), pp. 1905842(1-10).

Hao, J. Long, J. Li, B. Li, X. Zhang, S. Yang, F. & Guo, Z., 2019, "Toward high-performance hybrid Zn-based batteries via deeply understanding their mechanism and using electrolyte additive". *Advanced Functional Materials*, Vol. 29(34), pp. 1903605(1-9).

Karnchanawong, S. & Limpiteeprakan, P., 2009, "Evaluation of heavy metal leaching from spent household batteries disposed in municipal solid waste". *Waste Management*, Vol. 29(2), pp. 550-558.

Karden, E. Ploumen, S. Fricke, B. Miller, T. & Snyder, K., 2007, "Energy storage devices for future hybrid electric vehicles". *Journal of Power Sources*, Vol.168 (1), pp 2-11.

Li, H. Han, C. Huang, Y. Huang, Y. Zhu, M. Pei, Z. & Zhi, C., 2018, "An extremely safe and wearable solid-state zinc ion battery based on a hierarchical structured polymer electrolyte". *Energy & Environmental Science*, Vol.11 (4), pp. 941-951.

Li, Q., Zhu, S. & Lu, Y. 2017, "3D porous Cu current collector/Li-metal composite anode for stable lithium-metal batteries". *Advanced Functional Materials*, Vol. 27 (18), pp. 1606422 (1-8).

Luo, W. Gong, Y. Zhu, Y. Li, Y. Yao, Y. Zhang, Y., & Hu, L., 2017, "Reducing interfacial resistance between garnet-structured solid-state electrolyte and Li-metal anode by a germanium layer". *Advanced Materials*, Vol. 29 (22), pp. 1606042 (1-7).

M. Maccario, L. Croguennec, F. Weill, F. Le Cras, & Delmas, C., 2008, "C-containing $LiFePO_4$ materials—Part II: Electrochemical characterization". *Solid State Ionics*, Vol. 179 (40), pp. 2383-2389.

Panchal, S., 2016, “Experimental investigation and modeling of lithium-ion battery cells and packs for electric vehicles”. (Doctoral dissertation).

Parker, J. F. Chervin, C. N. Pala, I. R. Machler, M. Burz, M. F. Long, J. W. & Rolison, D. R., 2017, “Rechargeable nickel–3D zinc batteries: An energy-dense, safer alternative to lithium ion”. *Science*, Vol. 356(6336), pp. 415-418.

Sait Kursunoglu, Muammer, Kavya, Physicochemical, Probl. *Miner Process*. 50, 2014, pp. 39-53.

Sun, W. Wang, F. Hou, S. Yang, C. Fan, X. Ma, Z., & Wang, C., 2017, “Zn/MnO_2 battery chemistry with H^+ and Zn^{2+} coinsertion”. *Journal of the American Chemical Society*, Vol. 139(29), pp. 9775-9778.

Tran, M. K. Bhatti, A. Vrolyk, R. Wong, D. Panchal, S. Fowler, M. & Fraser, R., 2021, “A review of range extenders in battery electric vehicles: current progress and future perspectives”, *Journal of World Electric Vehicle*, Vol. 12 (2), pp. 54 (1-16).

Wan, F. Zhang, L. Dai, X. Wang, X. Niu, Z. & Chen, J., 2018, “Aqueous rechargeable zinc/sodium vanadate batteries with enhanced performance from simultaneous insertion of dual carriers”. *Nature Communications*, Vol. 9 (1), pp. 1-11.

Xará, S. M. Delgado, J. N. Almeida, M. F. & Costa, C. A., 2009, “Laboratory study on the leaching potential of spent alkaline batteries”. *Waste Management*, Vol. 29 (7), pp. 2121-2131.

Zhao, S., Han, B., Zhang, D., Huang, Q., Xiao, L., Chen, L. & Wei, W., 2018, “Unravelling the reaction chemistry and degradation mechanism in aqueous Zn/MnO_2 rechargeable batteries”. *Journal of Materials Chemistry A*, Vol. 6 (14), pp. 5733-5739.